Volume 1 | Number 1 | Jan 2013 | Pages 1–100

ChemComm

Chemical Communications
www.rsc.org/chemcomm

ROYAL SOCIETY OF CHEMISTRY

This is an *Accepted Manuscript*, which has been through the Royal Society of Chemistry peer review process and has been accepted for publication.

Accepted Manuscripts are published online shortly after acceptance, before technical editing, formatting and proof reading. Using this free service, authors can make their results available to the community, in citable form, before we publish the edited article. We will replace this *Accepted Manuscript* with the edited and formatted *Advance Article* as soon as it is available.

You can find more information about *Accepted Manuscripts* in the **Information for Authors**.

Please note that technical editing may introduce minor changes to the text and/or graphics, which may alter content. The journal's standard **Terms & Conditions** and the **Ethical guidelines** still apply. In no event shall the Royal Society of Chemistry be held responsible for any errors or omissions in this *Accepted Manuscript* or any consequences arising from the use of any information it contains.

www.rsc.org/chemcomm

Journal Name

A novel CO_2- and SO_2-tolerant dual phase composite membrane for oxygen separation

S. Cheng[a*], M. Søgaard[a], L. Han[a], W. Zhang[b], M. Chen[a], A. Kaiser[a] and P.V. Hendriksen[a]

A novel dual phase composite oxygen membrane ($Al_{0.02}Ga_{0.02}Zn_{0.96}O_{1.02}$ – $Gd_{0.1}Ce_{0.9}O_{1.95-\delta}$) was successfully prepared and tested. The membrane shows chemical stability against CO_2 and SO_2, and a stable oxygen permeation over 300 hours in CO_2 was demonstrated. ZnO is cheap and non-toxic and is therefore highly advantageous compared to other common materials used for the purpose.

Dense ceramic oxygen transport membranes (OTMs) can selectively separate oxygen from air at temperatures above 600 °C. The energy consumption of oxygen produced by OTMs can be significantly lower compared to conventional technologies such as cryogenic distillation or vacuum pressure swing adsorption, especially if the OTMs are thermally and/or chemically integrated with a high temperature process[1]. Main applications considered for OTMs include small scale oxygen production, oxygen for biomass gasification or oxy-fired cement plants, oxy-fuel combustion in power plants and partial oxidation of methane to synthesis gas[2]. In recent years, a significant number of papers have been dedicated to dual phase membranes, which consist of an ionic conductor and an electronic conductor[3-8]. Doped ceria or zirconia is normally used as the ionic conductor. Several different electronic conducting materials have been investigated for the purpose, including perovskite structured oxides[3,5], spinel structured oxides[7,9] and metals[8,10] (see Table S1 ESI†). Preferably the dual phase membranes should be tolerant against CO_2, which is particularly advantageous for a chemical integration of the membrane with a flue gas on the permeate side. Besides CO_2, one of the inevitable impurities arising from the combustion of sulfur-containing coals or biomass is SO_2. This corrosive gas can react quickly with most alkaline-earth doped perovskite based materials leading to reduced permeability due to the formation of alkaline earth sulphates.[11,12] Alkaline-earth elements should be avoided and stable performance in CO_2 or SO_2 containing atmospheres can be achieved. For example $NiFe_2O_4–Ce_{0.8}Tb_{0.2}O_{1.9}$ membrane shows good stability in CO_2- and SO_2- atmospheres[7]. The use of Ni, as well as Co and

Cr, which are preferred elements both for single phase and composite membranes, is problematic both in terms of the cost and due to their toxicity. It is therefore highly desirable to avoid these elements in an industrial manufacturing process. The development of a CO_2- and SO_2- stable membrane without expensive and toxic transition metals is therefore necessary for commercialization of OTMs.

Here we report on the use of doped ZnO with $Gd_{0.1}Ce_{0.9}O_{1.95-\delta}$ (GCO10) for high temperature oxygen transport membranes. ZnO offers the following advantages for the use in OTM: *i*) The electronic conductivity of ZnO is susceptible to tailoring *via* extrinsic doping. Doping of a slight amount of trivalent elements e.g. Al, Ga and In can drastically enhance the electronic conductivity of ZnO[13], rendering it a good electronic conductor. *ii*) ZnO is chemically stable in both CO_2 and SO_2 containing atmospheres. According to thermal dynamic calculation, decomposition of $ZnCO_3$ into ZnO and CO_2 occurs above 200 °C in air. A phase diagram (Fig. S3 ESI†) shows that the reaction between ZnO and SO_2 will only occur under high oxygen and sulfur dioxide partial pressures at low temperature. Typical conditions in an oxy-fuel power plant or cement plant would include SO_2 levels up to 100 ppm on the permeate side of the membrane. The chemical stability of ZnO should thereby meet the requirements for the membranes under the aforementioned conditions. *iii*) Furthermore, a ZnO dopant can enhance the electronic conductivity of the ceria itself over a wide range of temperature and oxygen partial pressure. It is found that this enhancement may occur without a sacrifice of ionic conductivity[14]. The grain boundary conductivity of GCO10 can even be enhanced by doping 1 mol % ZnO at low temperatures (< 500 °C)[15]. Schmale *et al.* reported that the electronic conductivity of Zn-doped ceria exhibits a striking jump when the concentration of ZnO is above 30 mol%, due to the formation of a ZnO-rich percolation network along the grain boundary[16]. *iv*) The thermal expansion coefficient (TEC) difference between ZnO (8×10^{-6} K^{-1} at 300 K[17]) and GCO10 (12×10^{-6} at 300 K-1273 K[18]) is moderate and therefore cracks between the micro grains of the two different phases can be avoided for suitable composite microstructures. *v*) Finally, zinc oxide is

non-toxic, abundant and inexpensive. ZnO based dual phase OTMs thus has numerous merits for the use in the commercialization of the technology.

The composite membrane investigated in the present study consists of 50 vol.% Al,Ga co-doped ZnO ($Al_{0.02}Ga_{0.02}Zn_{0.96}O_{1.02}$) and 50 vol.% $Gd_{0.1}Ce_{0.9}O_{1.95-\delta}$ (GCO10) (the composite is abbreviated AGZO-GCO55). $Al_{0.02}Ga_{0.02}Zn_{0.96}O_{1.02}$ and $Gd_{0.1}Ce_{0.9}O_{1.95-\delta}$ serve as electronic and oxide ion conducting phase, respectively. Fig. 1 displays the XRD patterns of GCO10, AGZO powder and crushed powder of a membrane sintered at 1200 °C. The reference XRD patterns of GCO10 and ZnO are also shown for comparison. According to Han *et al.*[19], doping small amount of Al and Ga into ZnO will not change the crystal structure. From the XRD patterns, it can be seen that the dual phase system merely consists of cubic fluorite structured GCO10 (space group 225: *Fm3m*) and hexagonal wurtzite structured AGZO (space group 186: *P63mc*). No secondary phases resulting from reactions could be detected within the resolution limit of the XRD, indicating sufficient mutual stability between GCO10 and AGZO. The crystal structure of the composite remains unaltered in the temperature range from 25 to 900 °C in air (Fig. S9 ESI†). XRD patterns of AGZO-GCO55 powders annealed in 100% CO_2 (flow=50 Nml min^{-1}) for 120 hours at 850 °C, shows that AGZO-GCO55 is chemically stable in CO_2 at high temperature. Also, identical XRD patterns for the powder before and after annealing in a SO_2 rich atmosphere indicate no formation of sulphate, whereas formation of $SrSO_4$ (Fig. S8 ESI†) is observed from a reference sample ($La_{0.6}Sr_{0.4}FeO_{3-\delta}-Gd_{0.1}Ce_{0.9}O_{1.95-\delta}$). This implies that AGZO-GCO55 with respect to SO_2 tolerability is superior to the Sr-containing perovskite. The results are also in good agreement with thermodynamic predictions (Fig. S3 ESI†).
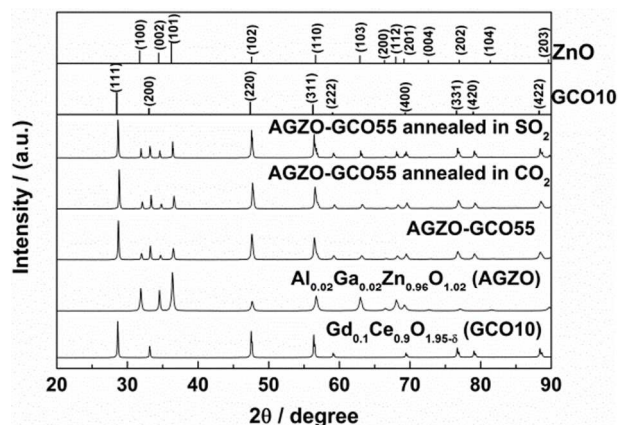

Fig.1 Normalized XRD patterns of dual phase AGZO-GCO55 membrane sintered at 1200 °C for 5 hours, sintered membrane annealed in 100% CO_2 for 120 hours and membrane annealed in SO_2 for 2 hours at 850°C. Diffraction patterns for single phase $Al_{0.02}Ga_{0.02}Zn_{0.96}O_{1.02}$ and $Gd_{0.1}Ce_{0.9}O_{1.95-\delta}$ are also shown.

Fig. 2 displays the scanning transmission electron microscopy (STEM) (See Fig.2a), EDX elemental mapping (Figs. 2b and 2c), EDX spectrum (Fig. 2d) and high resolution TEM (HR-TEM) image (Fig. 2e) of the crushed powder of the AGZO-GCO55 membrane. According to the Ce and Zn maps, GCO10 and AGZO grains are homogeneously distributed without any agglomeration of one phase and no obvious correlation of the Ce and Zn distribution could be observed, indicating no significant reaction between the grains or the formation of grain boundary layers.

By HRTEM imaging of the grain boundary between a GCO10 and a AGZO grain (Fig. 2e), the characteristic (111) GCO10 and (100) ZnO planes were identified on each side of the grain boundary. The presence of new phases could not be detected along the grain boundary.
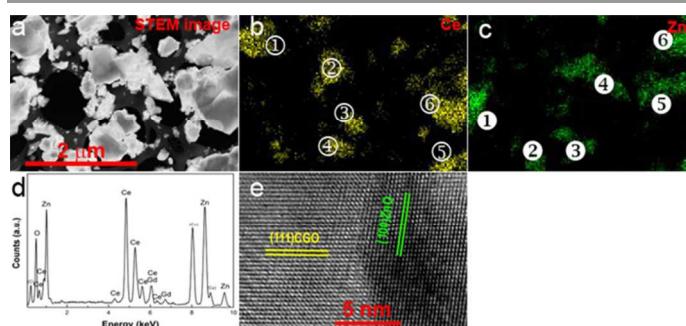

Fig. 2 a Bright-field STEM images of crushed powder of the membrane. EDX elemental maps of b. Cerium and c. Zinc. d. EDX spectrum. Cu/C comes from the carbon film/copper grid supporting for the powder. The symbols ①-⑥ and ❶-❻ represent different GCO10 and AGZO grains, respectively e. HRTEM image of a grain boundary contact in a dual phase membrane (GCO10 on the left and AGZO on the right).

Fig. 3 shows Arrhenius type plots of the oxygen permeation fluxes of a 1.1 mm thick GCO10 pellet coated with $La_{0.6}Sr_{0.4}CoO_{3-\delta}$ (LSC) layer and AGZO-GCO55 membranes with and without LSC coating measured with pure N_2 and CO_2 as sweep gas under a fixed oxygen partial pressure gradient ($\ln(pO_2'/pO_2'')$=5 and 8) in the temperature range between 600 °C and 1000 °C. LSC catalytic layers were used to ensure that the surface exchange reaction does not limit the flux. The flux data is also plotted for a fixed outlet flow (flow fixed over the temperature variation rather than fixing the driving force). Also, a calculated maximum flux for an ideal short circuited GCO10 and a pure GCO10 membrane (calculated based on the ionic conductivity and electronic conductivity from Ref.[20, 21]) under the same driving force is plotted for comparison. The uncertainty of the measured flux mainly originates from the uncertainty on the area of the membrane being tested and small leaks at the sealing (ESI† Table S1). Based on two nominally identical tests, the obtained results are clearly reproducible (Fig. S5 ESI†). Oxygen permeation fluxes for both sweep gases (N_2 and CO_2) show thermally activated feature with apparent activation energies (*E*a) of 74.5±2 kJmol^{-1} and 75.4±2 kJmol^{-1}, respectively. The almost equivalent oxygen flux observed under the same driving force conditions suggests that the prevailing rate limiting process is identical when using N_2 or CO_2 as sweep gas. In addition, the oxygen permeation flux measured using CO_2 as the sweep gas is slightly lower than that measured in N_2. "A slight suppression of the oxygen permeation flux in CO_2" when compared to N_2/He has also been found in other studies of OTMs.[22-26] The phenomenon is suggested to be a consequence of suppressed oxygen surface exchange rate due to the chemisorption of CO_2 on the surface of the activation layer with the occupation of oxygen vacancies by the oxide ions of CO_2[24]. On the other hand, the existence of a stagnant gas layer in the vicinity of the permeate side of OTMs has also been reported[27]. Such a stagnant gas layer can give rise to diffusion limitations at low oxygen partial pressures. The binary diffusion coefficient of oxygen in nitrogen ($D_{O_2-N_2}$= 0.75 cm^{2}s^{-1}) is slightly higher than that in carbon dioxide ($D_{O_2-CO_2}$=0.70 cm^{2}s^{-1}) at 900 °C. The different binary diffusion coefficients can therefore lead to different local oxygen partial pressures on the surface

of the permeate side and as consequence lead to slightly different oxygen fluxes even though the pO_2 of the effluent gas is identical.

The oxygen permeation flux of AGZO-GCO55 is ca. half of the calculated flux of short circuited GCO10 and two orders of magnitude higher than that measured for single phase GCO10. The enhanced oxygen flux of AGZO-GCO55 relative to GCO10 is due to the contribution of the n-type electronic conductivity originating from the percolating doped ZnO, as evidenced by the flux increase and the larger electrical conductivity (ESI† Fig.S6). The depressed flux of AGZO-GCO55 relative to short circuited GCO10 is ascribed to the partial blocking of the oxide ion paths by the AGZO and the more tortuous path for oxide ions, which is a general phenomenon observed in dual phase OTMs[3]. The membrane behaves as expected from the reported absence of chemical inter-reaction between the two phases simply as an ideal composite where naturally the addition of the electronic conductor takes up a volume otherwise available to ionic transport thus reducing the flux relative to ideally achievable in a pure ceria membrane. It is noted that the apparent activation energy of AGZO-GCO55 (74.5±2 kJ mol^{-1}) is slightly higher than that expected from the conductivity of GCO10 (66.1 kJ mol^{-1}). The larger apparent activation energy may originate from: i) a not insignificant contribution from the surface activation since the typical activation energy for a LSC electrode is 106 $kJmol^{-1}$.[28] ii) For the bulk diffusion, oxide ions will jump in the crystal structure of GCO10. The presence of ZnO surrounding GCO10 may result in strain effects or grain boundary effects that can possibly increase the energy barrier for oxide ion movement. Noticeably, the flux of a bare membrane is found to be more than one order of magnitude lower than that of the membrane with LSC activation layers. The lower flux and larger activation energy must be attributed to poor catalytic activity towards oxygen exchange of the composite AGZO-GCO55, which is consistent with the work on the use of ZnO as a SOFC electrode material[29]. It should be pointed out that the activation energy of the flux for a fixed flow of the effluent is 62 $kJmol^{-1}$, and thus lower than that measured under a fixed driving force. The lower activation energy is due to a continuous change of the driving force, as the oxygen permeating through the membrane reduces this with increasing temperature.
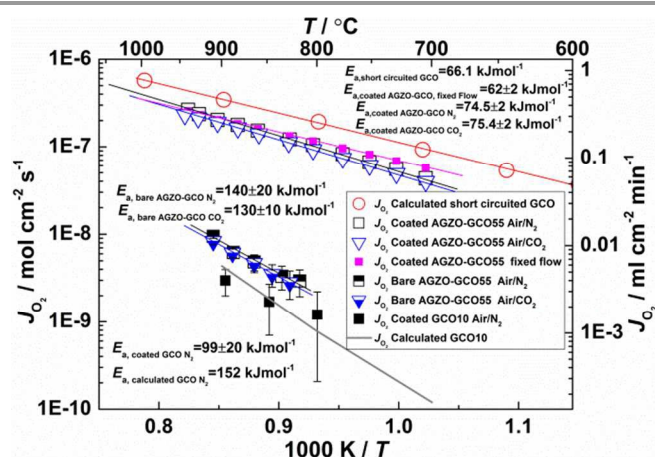

Fig.3 Arrhenius plot of the oxygen permeation flux (J_{O2}) of a GCO10 membrane with LSC coating and AGZO-GCO55 membranes with and without LSC activation layer measured in N_2 and CO_2 on the permeate side under a fixed driving force as a function of inverse temperature. The flux measured at fixed outlet flow is also plotted. For comparison the calculated flux of a short circuited membrane GCO10 is given (open circles).

The tested AGZO-GCO55 shows an oxygen permeation flux comparable to numerous ceria based dual phase membranes (ESI† Table S2). However, compared to most other systems studied in literature, the use of ZnO as the electronic conductor is advantageous due to its low cost and non-toxicity as previously stated. It is clear that future commercial membrane applications require significantly higher oxygen fluxes than reported here for 1.1 mm thick disks. A higher flux can be achieved by using a thin film membrane on a porous support structure. An additional advantage of the use of composites of GCO and ZnO is the possibility to tailor a thermal expansion coefficient of the composite to match that of cheap high toughness ceramics such as $Y_{0.03}Zr_{0.97}O_{1.985}$ (3YSZ) or mixtures of magnesia and alumina.

As shown in Fig. 4, the membrane flux was tracked for close to one month with N_2/CO_2 as the sweep gas at 860 °C followed by a measurement at 940 °C. The measurement was voluntarily terminated. A stable flux of 0.22 (STP) $mlcm^{-2} min^{-1}$ with N_2 as the sweep gas in the first 30 hours was observed. After switching the sweep gas to 100% CO_2, the flux decreases to 0.19 (STP) ml $cm^{-2} min^{-1}$ and levels off at 0.18 (STP) ml $cm^{-2} min^{-1}$ after 100 hours. After the sweep gas was switched back to 100% N_2, the flux effectively recovered to the initial level. The XRD patterns (Fig. S10 ESI†) of the feed and permeate side with the LSC activation layers before and after the measurement show no formation of new phases. No changes in the microstructure of the membrane layer itself compared to a fresh membrane could be observed after the 500 hour test (ESI† Fig.S11b). Also no microstructural changes of the feed side activation layer of LSC could be detected after test. The permeate side activation layer, however, showed a densified region (extending approximately 10 µm adjacent to the membrane) after test. EDS analysis (Fig.S12b ESI†) revealed the formation of a strontium rich layer along the interface between the activation layer and the membrane, which is ascribed to a reaction between $La_{0.6}Sr_{0.4}CoO_{3-\delta}$ and CO_2[25].
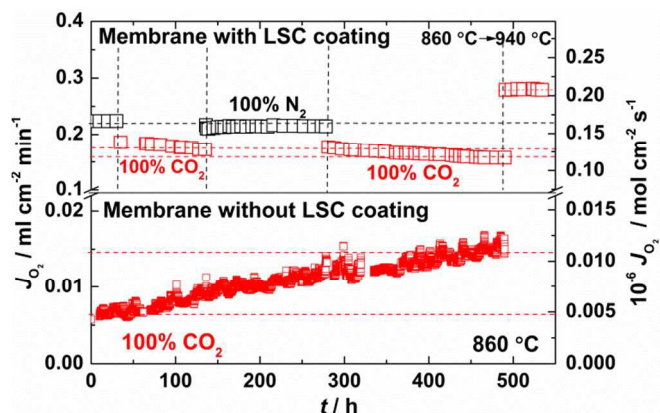

Fig.4 Oxygen permeation flux of AGZO-GCO55 dual phase membrane with and without LSC activation layer as a function of time at 860 °C and 940 °C. Feed gas: 100 ml min^{-1} air. Sweep gas: N_2 or CO_2 (total sweep gas flow: 150 N ml min^{-1}).

Over the 350 hours of test in CO_2 the flux through the coated membrane reduced by 7% with a tendency of a decreasing rate (Fig.S13 ESI†). Over a similar period (500 hours), the flux through an uncoated membrane (though much smaller) showed a clear increase (100%). This, together with the post-test microstructural findings, clearly shows that the dense membrane layer itself is chemically stable in CO_2, and that the decreasing flux observed for the coated membrane must be ascribed to

the catalyst layer on the permeate side. For most common membrane materials based on perovskite or similar structures, such as $Ba_{0.5}Sr_{0.5}Co_{0.8}Fe_{0.2}O_{3-\delta}$ (BSCF), the oxygen flux usually dramatically drops once CO_2 is introduced[23]. The dual phase AGZO-GCO55 membrane material studied here shows in contrast a relatively stable flux in CO_2. Further improved CO_2 stability can be expected if a more CO_2 stable electrocatalysts is used instead of LSC.

Conclusions

A novel CO_2 and SO_2 tolerant dual phase composite membrane material, consisting of 50 vol.% $Al_{0.02}Ga_{0.02}Zn_{0.96}O_{1.02}$ - 50 vol.% $Gd_{0.1}Ce_{0.9}O_{1.95-\delta}$ (AGZO-GCO55) was synthesized and tested as oxygen transport membrane. The total conductivity of the composite is mainly *n*-type electronic and originates from the percolating $Al_{0.02}Ga_{0.02}Zn_{0.96}O_{1.02}$ network. Fairly stable oxygen permeation in CO_2 could be proven in a 1.1 mm thick membrane for more than 500 hours at 860 °C and 940 °C. The AGZO-GCO55 composite material showed also sufficient stability in SO_2, making it a very good candidate for integration schemes of oxygen transport membrane into industrial applications that require direct contact with CO_2 and SO_2 containing environments.

Acknowledgments

Notes and references

1. M. Puig-Arnavat, S. Soprani, M. Sogaard, K. Engelbrecht, J. Ahrenfeldt, U. B. Henriksen and P. V. Hendriksen, *RSC Advances*, 2013, **3**, 20843-20854.
2. R. Bredesen, K. Jordal and O. Bolland, *Chem. Eng. Process. Process Intensif.*, 2004, **43**, 1129-1158.
3. A. J. Samson, M. Søgaard and P. V. Hendriksen, *J. Membr. Sci.*, 2014, **470**, 178-188.
4. B. Wang, J. Yi, L. Winnubst and C. Chen, *Journal of Membrane Science*, 2006, **286**, 22-25.
5. V. V. Kharton, A. V. Kovalevsky, A. P. Viskup, A. L. Shaula, F. M. Figueiredo, E. N. Naumovich and F. M. B. Marques, *Solid State Ionics*, 2003, **160**, 247-258.
6. X. Zhu and W. Yang, *AIChE Journal*, 2008, **54**, 665-672.
7. M. Balaguer, J. García-Fayos, C. Solís and J. M. Serra, *Chem. Mater.*, 2013, **25**, 4986-4993.
8. C. S. Chen, H. Kruidhof, H. J. M. Bouwmeester, H. Verweij and A. J. Burggraaf, *Solid State Ionics*, 1996, **86-88**, 569-572.
9. H. Luo, K. Efimov, H. Jiang, A. Feldhoff, H. Wang and J. Caro, *Angew. Chem. Int. Ed.*, 2011, **50**, 759-763.
10. E. Ruiz-Trejo, P. Boldrin, A. Lubin, F. Tariq, S. Fearn, R. Chater, S. N. Cook, A. Atkinson, R. I. Gruar, C. J. Tighe, J. Darr and N. P. Brandon, *Chem. Mater.*, 2014, **26**, 3887-3895.
11. J. Gao, L. Li, Z. Yin, J. Zhang, S. Lu and X. Tan, *Journal of Membrane Science*, 2014, **455**, 341-348.
12. S. Engels, T. Markus, M. Modigell and L. Singheiser, *Journal of Membrane Science*, 2011, **370**, 58-69.
13. T. Minami, *MRS Bulletin*, 2000, **25**, 38-44.
14. C. Chatzichristodoulou, P. V. Hendriksen, S. P. V. Foghmoes, S. Ricote, A. Kaiser, J. Classcock and S. Cheng. WO Pat.WO2014059992, 2014.
15. L. Ge, S. Li, Y. Zheng, M. Zhou, H. Chen and L. Guo, *J. Power Sources*, 2011, **196**, 6131-6137.
16. K. Schmale, M. Daniels, A. Buchheit, M. Grünebaum, L. Haase, S. Koops and H.-D. Wiemhöfer, *J. Electrochem. Soc.*, 2013, **160**, F1081-F1087.
17. H. Ibach, *Phys. Status Solidi (b)*, 1969, **33**, 257-265.
18. S. Wang, M. Katsuki, T. Hashimoto and M. Dokiya, *J. Electrochem. Soc.*, 2003, **150**, A952-A958.
19. L. Han, L. Hung, N. Nong, N. Pryds and S. Linderoth, *J. Electron. Mater.*, 2013, **42**, 1573-1581.
20. S. Wang, T. Kobayashi, M. Dokiya and T. Hashimoto, *J. Electrochem. Soc.*, 2000, **147**, 3606-3609.
21. C. Chatzichristodoulou and P. V. Hendriksen, *Physical Chemistry Chemical Physics*, 2011, **13**, 21558-21572.
22. W. Li, T.-F. Tian, F.-Y. Shi, Y.-S. Wang and C.-S. Chen, *Ind Eng Chem Res.* , 2009, **48**, 5789-5793.
23. K. Zhang, L. Liu, Z. Shao, R. Xu, J. C. Diniz da Costa, S. Wang and S. Liu, *J. Mater. Chem. A*, 2013, **1**, 9150-9156.
24. X. Tan, N. Liu, B. Meng, J. Sunarso, K. Zhang and S. Liu, *J. Membr. Sci.*, 2012, **389**, 216-222.
25. V. Esposito, M. Søgaard and P. V. Hendriksen, *Solid State Ionics*, 2012, **227**, 46-56.
26. H. Luo, H. Jiang, K. Efimov, F. Liang, H. Wang and J. Caro, *Ind. Eng. Chem. Res.*, 2011, **50**, 13508-13517.
27. M. Søgaard, Technical University of Denmark, PhD thesis, 2006.
28. P. Hjalmarsson, M. B. Mogensen and M. Søgaard, *Solid State Ionics*, 2008, **179**, 1422-1426.
29. H. J. Park and S. Kim, *Electrochemical and Solid-State Letters*, 2007, **10**, B187-B190.